

Impact of Bi_2O_3 on the X-ray shielding characteristics of telluro-borate-bismuth glass for medical applications

Bonginkosi Vincent Kheswa* , Siyabonga Ntokozo Thandoluhle Majola 

Department of Physics, University of Johannesburg, Doornfontein, South Africa.

*Corresponding author: vincentk@uj.ac.za

Original Research

Abstract:

Received:
25 February 2024
Revised:
31 March 2024
Accepted:
7 May 2024
Published online:
25 May 2024

The study of lead-free glasses for radiation shielding applications has drawn global attention. This work aimed to theoretically investigate the impact of Bi_2O_3 on X-ray shielding characteristics of telluro-borate-bismuth glass samples, in the 15 – 300 keV energy region. Sample S5 ($55\text{Bi}_2\text{O}_3 - 5\text{TeO}_2 - 20\text{SrO} - 5\text{ZnO} - 15\text{Bi}_2\text{O}_3$) yielded highest *LAC*, *MAC*, and Z_{eff} ($1.066 - 252.061 \text{ cm}^{-1}$, $0.249 - 58.893 \text{ cm}^2/\text{g}$, and $67.81 - 30.16$), alongside the lowest *HVL*, *TVL*, and *MFP* ($0.003 - 0.650 \text{ cm}$, $0.009 - 2.160 \text{ cm}$, and $0.004 - 0.938 \text{ cm}$). Hence, S5 emerged as the most effective X-ray shielding glass among the samples studied.

© The Author(s) 2024

Keywords: X-ray shielding; Telluro-borate-bismuth; Bi_2O_3 ; Phy-X/PSD; XCOM

1. Introduction

X-rays, falling within the energy range of a few eV to hundreds of keV, are ionizing electromagnetic waves that can be generated as bremsstrahlung radiation or characteristic X-rays. Their diverse industrial applications encompass computed tomography scans, dental X-rays, screening freight trains and luggage, power plant fluid supply pipe maintenance, and detecting foreign objects in food. However, without proper shielding, the hazardous nature of X-rays poses health risks to individuals working in these industries. There are various materials suitable for X-ray shielding, with lead-based options being one of the traditional choices. However, the toxicity of lead diminishes its user-friendliness, despite its effectiveness owing to high electron density and linear attenuation coefficient for photons [1]. Consequently, global research interest is focused on finding non-toxic lead-free glass materials for X-ray and γ -ray shielding [2–11]. For instance, a recent comprehensive study [12] highlighted the superior X-ray shielding properties of Sm^{3+} -doped bismuth-borate glass compared to those doped with Nd^{3+} and Ce^{3+} . Similarly, a computational investigation by Ref. [13] explored the X-ray shielding characteristics of $\text{Bi}_2\text{O}_3 - \text{B}_2\text{O}_3 - \text{TeO}_2 - \text{TiO}_2$ glass in the

dental diagnostic energy range (30 to 80 keV), suggesting its potential use in protective masks during oral cavity diagnostic irradiation. Additionally, Ref. [14] examined the photon shielding properties of $\text{Li}_2\text{O} - \text{B}_2\text{O}_3 - \text{MgO} - \text{Er}_2\text{O}_3$ glass, demonstrating improvement with increased Sm_2O_3 content. In a parallel study [15], the X-ray shielding capacity of $\text{La}_2\text{O}_3 - \text{CaO} - \text{B}_2\text{O}_3 - \text{SiO}_3$ glass was investigated, revealing enhanced effectiveness with higher La_2O_3 content. In a similar vein, Refs. [16–22] recently scrutinized the radiation shielding properties of various borate glass systems. Their findings revealed that incorporating Cr_2O_3 , TeO_2 , Gd_2O_3 , WO_3 , $\text{TeO}_2/\text{MoO}_3$, and CeO_2 improved the X-ray and γ -ray shielding capabilities of Cr_2O_3 -doped borosilicate, TeO_2 -doped borosilicate, Gd_2O_3 -doped alumina borate, $\text{B}_2\text{O}_3 - \text{PbO} - \text{TeO}_2 - \text{CeO}_2 - \text{WO}_3$, $\text{TeO}_2 - \text{B}_2\text{O}_3 - \text{Li}_2\text{O} - \text{MoO}_3 - \text{CuO}$, and CeO_2/sand reinforced borate glasses, respectively. Additionally, the $34\text{TeO}_2 - 35\text{B}_2\text{O}_3 - 30\text{PbO} - 1\text{V}_2\text{O}_5$ glass exhibited the best photon shielding characteristics among the studied $\text{TeO}_2 - \text{BaO} - \text{B}_2\text{O}_3 - \text{PbO} - \text{V}_2\text{O}_5$ samples.

In a recent synthesis effort detailed by Ref. [23], a unique set of telluro-borate-bismuth glass samples was manufactured using the melt-quenching technique. However, the examination of their radiation shielding properties has been

limited to the photon energy of 511 keV. This study addresses this gap by investigating their X-ray shielding characteristics in the X-ray energy region below 300 keV, particularly significant for applications such as dental diagnoses, and computed tomography scans. In particular, the current work provides a detailed study of the impact of Bi₂O₃ concentration on the X-ray shielding properties of (70-x)B₂O₃ - 5TeO₂ - 20SrO - 5ZnO - (x)Bi₂O₃, where x = 0, 1, 5, 10, and 15 mol%, across the 15 keV to 300 keV photon energy range using the Phy-X/PSD and XCOM simulation software.

2. Methods

The X-ray attenuation characteristics of the 70B₂O₃ + 5TeO₂ + 20SrO + 5ZnO, 69B₂O₃ + 5TeO₂ + 20SrO + 5ZnO + Bi₂O₃, 65B₂O₃ + 5TeO₂ + 20SrO + 5ZnO + 5Bi₂O₃, 60B₂O₃ + 5TeO₂ + 20SrO + 5ZnO + 10Bi₂O₃, and 55B₂O₃ + 5TeO₂ + 20SrO + 5ZnO + 15Bi₂O₃ glass samples were computationally investigated using the Phy-X/PSD simulation software. Phy-X/PSD, a simulation package designed for user-friendly operation, is utilized remotely on the Ubuntu operating system [24, 25]. It specializes in computing radiation shielding properties, namely *MAC*, *LAC*, *HVT*, *TVT*, *MFP*, and *Z_{eff}*, within the photon energy range of 1 keV to 100 GeV. In contrast, the XCOM software, used for validation of Phy-X/PSD results, focuses solely on *MAC* calculations within the same photon energy range [26], but this *MAC* was converted to *LAC* using the densities of the samples. These simulation packages are based on the principles discussed below and have been rigorously tested in the literature.

The mass attenuation coefficient (*MAC*) and linear attenuation coefficient (μ) characterize the probability of interaction between X-rays and a material used for radiation shielding. The linear attenuation coefficient is linked to photon intensity and the absorber's thickness, denoted as *x*, according to [25]

$$I_f = I_i \exp(-\mu x) \quad (1)$$

where *I_i* and *I_f* are initial and attenuated photon intensities, respectively. High values of μ indicate superior radiation shielding capability. All other radiation shielding properties are derived from μ . Specifically, the mass attenuation coefficient (*MAC*) is calculated from the linear attenuation coefficient (μ) and the density (ρ) of the absorber using [25]

$$MAC = \frac{\mu}{\rho} \quad (2)$$

In the same vein, the effective atomic number of a material is calculated from the mass attenuation coefficients of the constituents using the following expression [25].

$$Z_{eff} = \frac{\sum_j f_j A_j \left(\frac{\mu}{\rho}\right)_j}{\sum_j \frac{f_j A_j}{Z_j} \left(\frac{\mu}{\rho}\right)_j} \quad (3)$$

where *f_j*, *A_j*, and *Z_j* are used to denote the mole fraction, atomic weight, and atomic number of each element in the sample, respectively.

Moreover, the half-value thickness (*HVT*) and tenth-value thickness (*TVT*), indicating the thicknesses needed to attenuate photons by 50% and 90%, are expressed as [25]:

$$HVT = \frac{\ln 2}{\mu} \quad (4)$$

and

$$TVT = \frac{\ln 10}{\mu} \quad (5)$$

Smaller *HVT* and *TVT* values signify better radiation shielding material for X-rays. Furthermore, the mean free path (*MFP*) defines the average distance between two consecutive interactions of a photon with the absorber material and is correlated with the linear attenuation coefficient (μ) through the subsequent expression [25].

$$MFP = \frac{1}{\mu} \quad (6)$$

A material demonstrates higher efficiency in shielding electromagnetic radiation when its mean-free path (*MFP*) is lower.

Tables 1 and 2 show the summary of input data used in the Phy-X/PSD and XCOM calculations for our glass samples S1, S2, S3, S4, and S5.

3. Results and discussions

In this section, we delve into the discussion of our findings concerning the linear attenuation coefficient (*LAC*), mass attenuation coefficient (*MAC*), effective atomic number (*Z_{eff}*), half-value thickness (*HVT*), tenth-value thickness (*TVT*), and mean-free path (*MFP*) for the glass samples S1, S2, S3, S4, and S5. Figure 1 shows the linear attenuation coefficient of the samples S1, S2, S3, S4, and S5 in the 15 keV to 300 keV photon energy range. The results demonstrate a rapid decrease in the linear attenuation coefficient (*LAC*) as X-ray energy increases for all five glass materials, a trend consistent with existing literature [3, 27, 28]. This phenomenon is attributed to the dominance

Table 1. Molecular composition (mol%) of glass samples for Phy-X/PSD calculations [23].

Code	B ₂ O ₃	TeO ₂	SrO	ZnO	Bi ₂ O ₃	Density (g/cm ³)
S1	70	5	20	5	-	2.9
S2	69	5	20	5	1	3
S3	65	5	20	5	5	3.41
S4	60	5	20	5	10	3.92
S5	55	5	20	5	15	4.28

Table 2. Chemical composition (wt%) of glass samples for XCOM calculations.

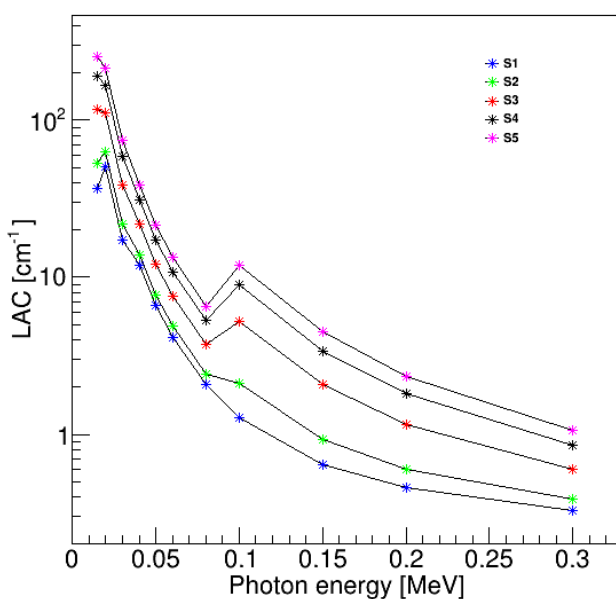
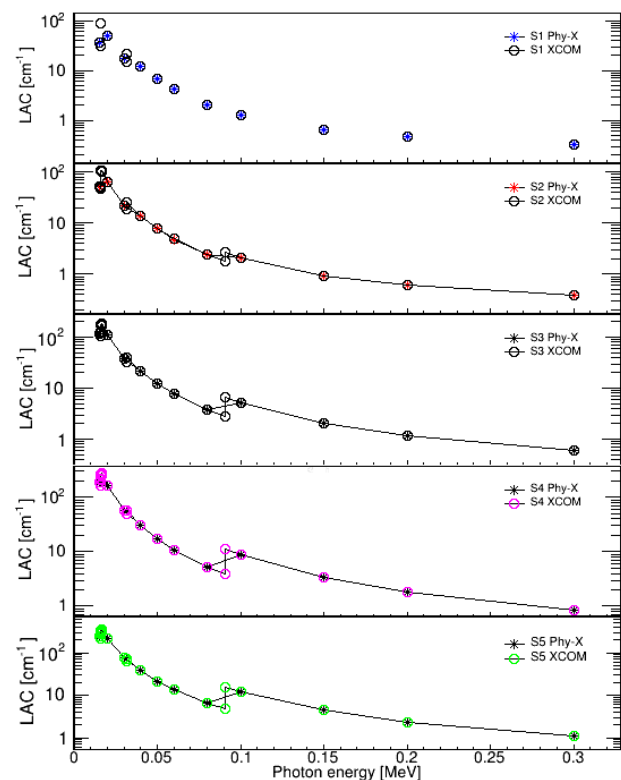
Code	B ₂ O ₃	TeO ₂	SrO	ZnO	Bi ₂ O ₃	Density (g/cm ³)
S1	0.6	0.1	0.25	0.05	-	2.9
S2	0.56	0.09	0.24	0.05	0.06	3
S3	0.45	0.08	0.21	0.04	0.23	3.41
S4	0.35	0.07	0.17	0.03	0.39	3.92
S5	0.27	0.06	0.15	0.03	0.5	4.28

of the photoelectric absorption component in this energy range, which sharply decreases with an increase in photon energy. Among the five glasses, S5 which has the highest Bi₂O₃ content exhibits the highest *LAC* at all energies, while S1 which has the lowest Bi₂O₃ content has the lowest *LAC*. Specifically, the *LAC* ranges from 1.066 to 252.061 cm⁻¹ for S5 and 0.331 to 50.827 cm⁻¹ for S1. Notably, there is a sudden surge in the *LAC* at 100 keV for samples S2, S3, S4, and S5, attributed to the *K*-absorption edge which is due to the presence of Bi₂O₃ in systems and intensifying the photoelectric absorption. A similar enhancement is observed at 20 keV in samples S1 and S2. It corresponds to the *K*-absorption edge that does not originate from the presence of Bi₂O₃, as it is observed even in S1 which does not contain Bi₂O₃.

To validate the Phy-X/PSD calculation, we compared the Phy-X/PSD and XCOM results. The comparison of *LAC* values, computed using Phy-X/PSD and XCOM, is presented in Figure 2. Remarkably, both simulation tools exhibit excellent agreement, instilling confidence in the accuracy of the calculated *LAC* values across all five glass samples. Numerous other research endeavors have also conducted comprehensive assessments of these simulation programs in the literature, specifically within the realm of various heavy-metal oxide glasses, including those featuring bismuth. Noteworthy is their validation through extensive

comparisons with experimental data and Monte Carlo simulations conducted using numerical codes such as MCNP [20, 29–31]. Thus, the reliability of the outcomes derived from Phy-X/PSD and XCOM is further affirmed. For the remaining radiation shielding parameters, our focus is on results derived using Phy-X/PSD only, as they build upon the validated *LAC*, and there is no need to further validate them.

The mass attenuation coefficient of all five samples is depicted in Figure 3. It has the same shape as the *LAC*. This is consistent with the relation of the two quantities provided in Equation (2). There is an enhancement in the *MAC* with an increase in the Bi₂O₃ content. In detail, It is in the ranges of 0.114 to 17.527 cm²/g, 0.129 to 17.755 cm²/g, 0.177 to 34.106 cm²/g, 0.219 to 48.527 cm²/g, and 0.249 to 58.893 cm²/g for samples S1, S2, S3, S4, and S5, respectively. Hence, sample S1 has the lowest *MAC* in the whole X-ray energy region, while S5 which has the highest content of Bi₂O₃ has the highest *MAC*. Results similar to these have been reported on different glass materials in the literature

**Figure 1.** Linear attenuation coefficient of S1, S2, S3, S4, and S5.**Figure 2.** Comparison of the Phy-X/PSD and XCOM linear attenuation coefficients.

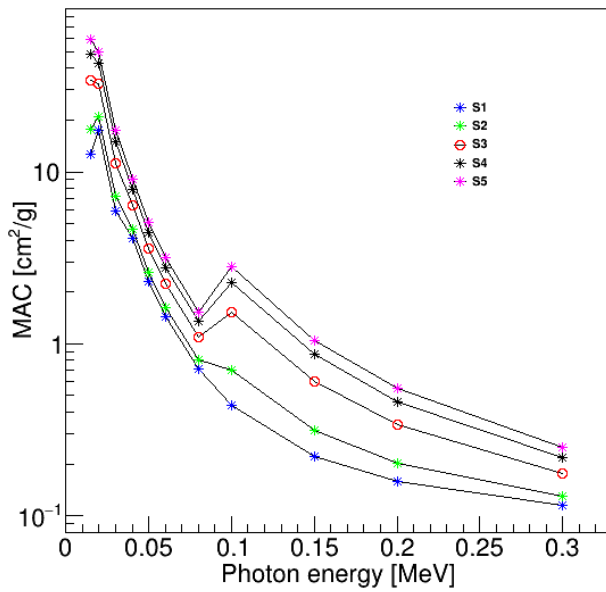


Figure 3. Mass attenuation coefficient of S1, S2, S3, S4, and S5.

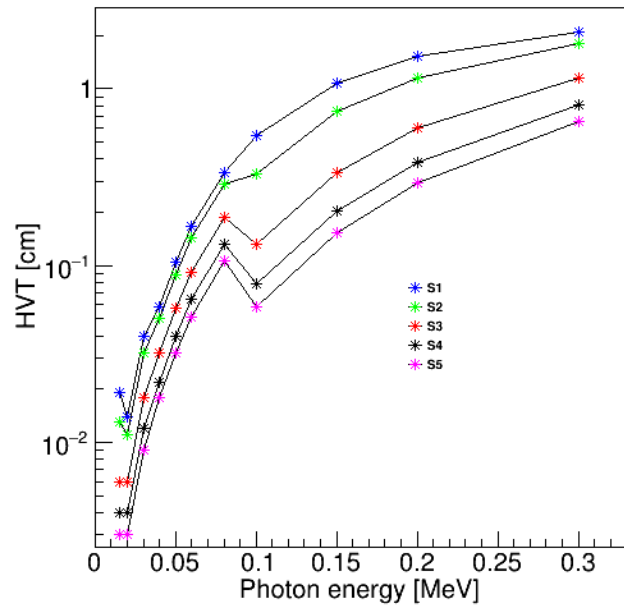


Figure 5. Half-value thickness of S1, S2, S3, S4, and S5.

[16, 32]. For instance, Ref. [16] showed theoretically and experimentally that increasing the content of Cr_2O_3 in a borosilicate glass system results in the enhancement in the mass attenuation coefficient of the borosilicate glass, and the sample with the highest concentration of Cr_2O_3 has the highest MAC.

The distribution of the effective atomic number (Z_{eff}) for all five glass materials within the 15 – 300 keV photon energy range is presented in Figure 4. The Z_{eff} ranges between 35.34 and 10.20, 39.17 and 11.87, 53.82 and 17.97, 63.00 and 24.54, and 67.82 and 30.16 for S1, S2, S3, S4 and S5 glasses, respectively. Clearly, Z_{eff} improves with an increase in the Bi_2O_3 concentration, and sample S5, which has the highest Bi_2O_3 content, has the highest Z_{eff} in the

whole 15 to 300 keV energy range. A trend similar to this one has been seen in other studies [21, 22]. In this study, it corresponds to the high atomic number (Z) of Bi, which leads to the rapid rise of the photo-absorption cross-section with an increase in the Bi_2O_3 concentration, and thus increases the effective atomic number of the glass. Furthermore, Z_{eff} of S1 shows a sudden increase at 20 keV and 40 keV, beyond which it decreases fast as the X-ray energy increases towards 150 keV, and declines relatively slowly as the photon energy increases from 150 keV to 300 keV. A similar trend is observed in the Z_{eff} of S2 except that it has another rise and fall at 100 keV. On the other hand, the effective atomic number of S3, S4, and S5 decreases fast as the X-ray energy increases from 15 keV to 80 keV, and it suddenly increases at 100 keV after which it

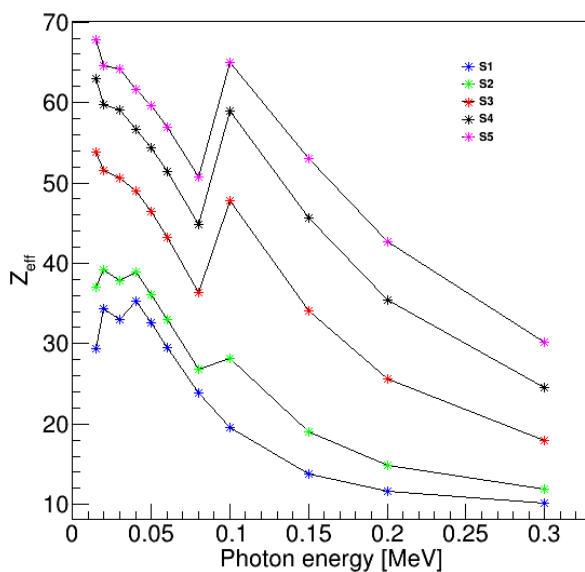


Figure 4. Effective atomic number of S1, S2, S3, S4, and S5.

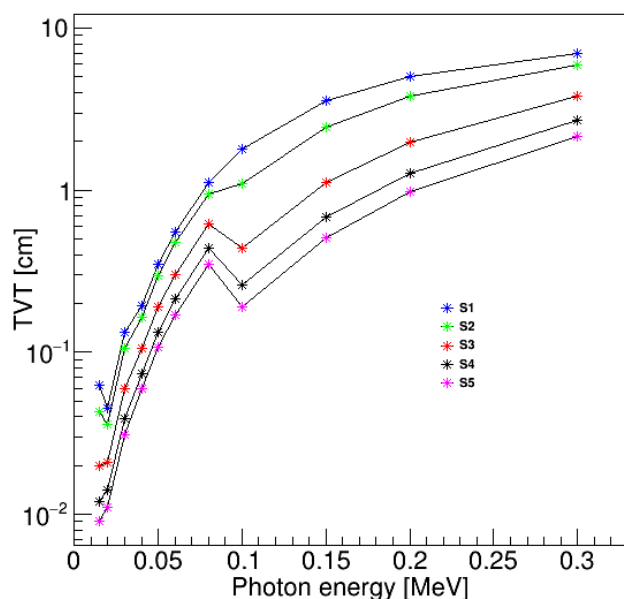


Figure 6. Tenth-value thickness of S1, S2, S3, S4, and S5.

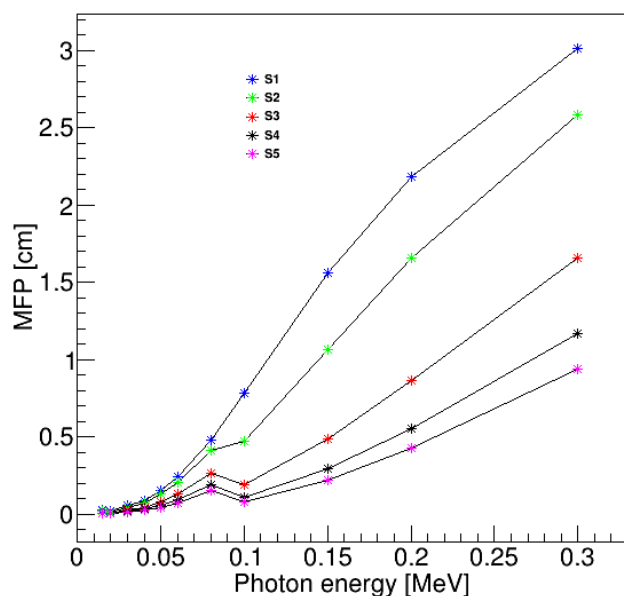


Figure 7. Mean-free path of S1, S2, S3, S4, and S5.

continues to decrease rapidly as the photon energy increases towards 300 keV. The enhancements of Z_{eff} at 20, 40, and 100 keV are due to the K -absorption edges, as discussed above. These structures are expected on the effective atomic number because they are observed in the mass attenuation coefficient, as well, which is the input data for the calculation of Z_{eff} (see Equation (3)). The reduction of Z_{eff} with photon energy is attributed to the reduction in the photoelectric cross-sections that occurs as the energy increases.

The computed HVT and TVT for S1, S2, S3, S4, and S5 are illustrated in Figures 5 and 6. We observe that these quantities show the same trend. This is consistent with the fact that they both depend on the same parameter, the linear attenuation coefficient (see Equations (4) and (5)). There is also an increase in HVT and TVT with a corresponding rise in photon energy, and S5, which has the highest mol% of Bi_2O_3 remains the lowest in the entire X-ray energy range; This observation is consistent with other findings in the literature [32–34]. In detail, the HVT of samples S1, S2, S3, S4, and S5 is in the range of 0.014 to 2.091 cm, 0.011 to 1.790 cm, 0.006 to 1.150 cm, 0.004 to 0.808 cm, and 0.003 to 0.650 cm, respectively. The TVT ranges from 0.045 to 6.947 cm, 0.036 to 5.945 cm, 0.020 to 3.820 cm, 0.012 to 2.684 cm, and 0.009 to 2.160 cm for S1, S2, S3, S4, and S5, respectively. Furthermore, we observe a sharp reduction in HVT and TVT of S1 and S2 at 20 keV above which they, on average, rise fast with an increase in the X-ray energy as it approaches 150 keV, beyond which they rise gradually as the photon energy increases towards 300 keV. On the other hand, the HVT and TVT of S3, S4, and S5 increase rapidly as the photon energy increases from 15 keV to 80 keV. At 100 keV they abruptly decline and continue rising as the X-ray energy approaches 300 keV. The sharp reductions in HVT and TVT at 20 keV and 100 keV are due to the K -edge electrons, which enhance the photo-absorption component of the linear attenuation coefficient (LAC), and thus, decrease the HVT and TVT which are inversely pro-

portional to LAC (see Equations (4) and (5)).

Figure 7 depicts the variation of the mean free path (MFP) for our five glass samples with X-ray energy. The trend is evident: the MFP increases as photon energy rises, and S5 consistently maintains the lowest MFP across the entire X-ray energy range, while S1 remains the highest. In particular, the MFP of S1, S2, S3, S4, and S5 is between 0.020 and 3.017 cm, 0.016 and 2.582 cm, 0.009 and 1.659 cm, 0.005 and 1.166 cm, and 0.004 and 0.938 cm, respectively. The increase in MFP with photon energy aligns with observations in the literature [35, 36]. The reduction in the MFP with an increase in Bi_2O_3 concentration is attributed to the corresponding rise in the density of additional electrons, which are mostly contributed by high Z bismuth atoms. Furthermore, the significant contribution of the K -edge electrons in the reduction of the MFP is observed in samples S3, S4, and S5 at 100 keV.

4. Conclusion

The X-ray shielding properties of $(70-x)B_2O_3 - 5TeO_2 - 20SrO - 5ZnO - (x)Bi_2O_3$, where $x = 0, 1, 5, 10,$ and 15 mol%, glass system were investigated using the Phy-X/PSD simulation software, and validated using XCOM. The findings revealed that sample $55B_2O_3 - 5TeO_2 - 20SrO - 5ZnO - 15Bi_2O_3$ exhibited the highest values for LAC , MAC , and Z_{eff} , ranging respectively from 1.066 to 252.061 cm^{-1} , 0.249 to $58.893\text{ cm}^2/\text{g}$, and 67.81 to 30.16. Additionally, it demonstrated the lowest HVL , TVL , and MFP , spanning from 0.003 to 0.650 cm, 0.009 to 2.160 cm, and 0.004 to 0.938 cm, respectively. Consequently, S5 emerged as the most efficient X-ray shielding glass among the samples studied. Thus, S5 has the potential to be used as an X-ray shielding glass in medical applications.

Acknowledgement

Authors would like to acknowledge funding under research grant numbers CSR2204214088 and SRUG220317100.

Authors Contributions

The authors did all simulations, data analysis, and compilation of the manuscript.

Availability of data and materials

The datasets generated and analyzed during the current study are available from the corresponding author upon reasonable request.

Conflict of Interests

The author declare that they have no known competing financial interests or personal relationships that could have appeared to influence the work reported in this paper.

Open Access

This article is licensed under a Creative Commons Attribution 4.0 International License, which permits use, sharing, adaptation, distribution and

reproduction in any medium or format, as long as you give appropriate credit to the original author(s) and the source, provide a link to the Creative Commons license, and indicate if changes were made. The images or other third party material in this article are included in the article's Creative Commons license, unless indicated otherwise in a credit line to the material. If material is not included in the article's Creative Commons license and your intended use is not permitted by statutory regulation or exceeds the permitted use, you will need to obtain permission directly from the OICC Press publisher. To view a copy of this license, visit <https://creativecommons.org/licenses/by/4.0>.

References

- [1] R. C. Klein and C. Weilandics. "Potential health hazards from lead shielding.". *American Industrial Hygiene Association Journal*, **57**:1124–1126, 1996. DOI: <https://doi.org/10.1080/15428119691014215>.
- [2] H. O. Tekin, G. AlMisned, H. M. H. Zakaly, A. Zamil, D. Khoucheich, G. Bilal, L. Al-Sammaraie, S. A. M. Issa, M. S. Al-Buriahi, and A. Ene. "Gamma, neutron, and heavy charged ion shielding properties of Er³⁺-doped and Sm³⁺-doped zinc borate glasses.". *Open Chemistry*, **20**:130–145, 2022. DOI: <https://doi.org/10.1515/chem-2022-0128>.
- [3] E. S. A. Waly, M. A. Fusco, and M. A. Bourham. "Gamma-ray mass attenuation coefficient and half value layer factor of some oxide glass shielding materials.". *Annals of Nuclear Energy*, **96**:26–30, 2016. DOI: <https://doi.org/10.1016/j.anucene.2016.05.028>.
- [4] G. AlMisned, W. Elshami, S. Issa, G. Susoy, H. Zakaly, M. Algethami, Y. S. Rammah, A. Ene, S. A. Al-Ghamdi, A. A. Ibraheem, and H. O. Tekin. "Enhancement of Gamma-ray shielding properties in cobalt-doped heavy metal borate glasses: The role of lanthanum oxide reinforcement.". *Materials*, **14**:7703, 2021. DOI: <https://doi.org/10.3390/ma14247703>.
- [5] S. Kaur and K. Singh. "Investigation of lead borate glasses doped with aluminium oxide as gamma ray shielding materials.". *Annals of Nuclear Energy*, **63**:350–354, 2014. DOI: <https://doi.org/10.1016/j.anucene.2013.08.012>.
- [6] I. Akkurt, R. B. Malidarre, and T. Kavas. "Monte Carlo simulation of radiation shielding properties of the glass system containing Bi₂O₃". *European Physical Journal Plus*, **136**:264, 2021. DOI: <https://doi.org/10.1140/epjp/s13360-021-01260-y>.
- [7] M. Sayyed, B. Elbashir, H. Tekin, E. Altunsoy, and D. Gaikwad. "Radiation shielding properties of pentatertiary borate glasses using MCNPX code.". *Journal of Physics and Chemistry of Solids*, **121**:17–21, 2018. DOI: <https://doi.org/10.1016/j.jpics.2018.05.009>.
- [8] P. Sopapan, J. Laopaiboon, O. Jaiboon, C. Yenchai, and R. Laopaiboon. "Feasibility study of recycled CRT glass on elastic and radiation shielding properties used as X-ray and gamma-ray shielding materials.". *Progress in Nuclear Energy*, **119**:103149, 2020. DOI: <https://doi.org/10.1016/j.pnucene.2019.103149>.
- [9] M. Sayyed, E. M. Çelikbilek, A. E. Ersundu, G. Lakshminarayana, and P. Kostka. "Investigation of radiation shielding properties for MeOPbCl₂ - TeO₂ (MeO = Bi₂O₃, MoO₃, Sb₂O₃, WO₃, ZnO) glasses.". *Radiation Physics and Chemistry*, **144**:419–425, 2018. DOI: <https://doi.org/10.1016/j.radphyschem.2017.10.005>.
- [10] J. Kaewkhao, A. Pokaipisit, and P. Limsuwan. "Study on borate glass system containing with Bi₂O₃ and BaO for gamma-rays shielding materials: Comparison with PbO.". *Journal of Nuclear Materials*, **399**:38–40, 2010. DOI: <https://doi.org/10.1016/j.jnucmat.2009.12.020>.
- [11] N. Chanthima, J. Kaewkhao, P. Limkitjaroenporn, S. Tuscharoen, S. Kothan, M. Tungjai, S. Kaewjaeng, S. Sarachai, and P. Limsuwan. "Development of BaO - ZnO - B₂O₃ glasses as a radiation shielding material.". *Radiation Physics and Chemistry*, **137**:72–77, 2017. DOI: <https://doi.org/10.1016/j.radphyschem.2016.03.015>.
- [12] B. V. Kheswa. "X-ray shielding properties of bismuth-borate glass doped with rare-earth ions.". *Open Chemistry*, **21**:20220345, 2023. DOI: <https://doi.org/10.1515/chem-2022-0345>.
- [13] Y. Al-Hadeethi, M. I. Sayyed, H. Mohammed, and L. Rimondini. "X-ray photons attenuation characteristics for two tellurite based glass systems at dental diagnostic energies.". *Ceramics International*, **46**:251–257, 2020. DOI: <https://doi.org/10.1016/j.ceramint.2019.08.258>.
- [14] M. H. A. Mhareb. "Physical, optical and shielding features of Li₂O - B₂O₃ - MgO - Er₂O₃ glasses codoped of Sm₂O₃". *Applied Physics A*, **126**:71, 2020. DOI: <https://doi.org/10.1007/s00339-019-3262-9>.
- [15] S. Kaewjaeng, S. Kothan, W. Chaiphaksa, N. Chanthima, R. Rajaramakrishna, H. Kim, and J. Kaewkhao. "High transparency La₂O₃ - CaOB₂O₃ - SiO₂ glass for diagnosis X-ray shielding material application.". *Radiation Physics and Chemistry*, **160**:41–47, 2019. DOI: <https://doi.org/10.1016/j.radphyschem.2019.03.018>.
- [16] B. Aktas, S. Yalcin, K. Dogru, Z. Uzunoglu, and D. Yilmaz. "Structural and radiation shielding properties of chromium oxide doped borosilicate glass.". *Radiation Physics and Chemistry*, **156**:144–149, 2019. DOI: <https://doi.org/10.1016/j.radphyschem.2018.11.012>.
- [17] B. Aktas, A. Acikgoz, D. Yilmaz, S. Yalcin, K. Dogru, and N. Yorulmaz. "The role of TeO₂ insertion on the radiation shielding, structural and physical properties of borosilicate glasses.". *Journal*

- of *Nuclear Materials*, **563**:153619, 2022. DOI: <https://doi.org/10.1016/j.jnucmat.2022.153619>.
- [18] M. Fidan, A. Acikgoz, G. Demircan, D. Yilmaz, and B. Aktas. “Optical, structural, physical, and nuclear shielding properties, and albedo parameters of $\text{TeO}_2\text{-BaO-B}_2\text{O}_3\text{-PbO-V}_2\text{O}_5$ glasses.”. *Journal of Physics and Chemistry of Solids*, **163**:110543, 2022. DOI: <https://doi.org/10.1016/j.jpics.2021.110543>.
- [19] B. B. Solak, B. Aktas, D. Yilmaz, S. Kalecik, S. Yalcin, A. Acikgoz, and G. Demircan. “Exploring the radiation shielding properties of $\text{B}_2\text{O}_3\text{-PbO-TeO}_2\text{-CeO}_2\text{-WO}_3$ glasses: A comprehensive study on structural, mechanical, gamma, and neutron attenuation characteristics.”. *Materials Chemistry and Physics*, **312**:128672, 2024. DOI: <https://doi.org/10.1016/j.matchemphys.2023.128672>.
- [20] N. Yorulmaz, M. M. Yasar, A. Acikgoz, Y. Kavun, G. Demircan, M. Kamislioglu, B. Aktas, and E. O. Ulas. “Influence of Gd_2O_3 on structural, optical, radiation shielding, and mechanical properties of borate glasses.”. *Optical Materials*, **149**:115032, 2024. DOI: <https://doi.org/10.1016/j.optmat.2024.115032>.
- [21] M. Fidan, A. Acikgoz, D. Yilmaz, G. Demircan, S. Kalecik, B. Aktas, and S. Isgor. “Investigation of the structural, mechanical, radiation and neutron shielding properties of the $\text{TeO}_2\text{-B}_2\text{O}_3\text{-Li}_2\text{O-MoO}_3\text{-CuO}$ glass system.”. *Journal of Alloys and Compounds*, **976**:172981, 2024. DOI: <https://doi.org/10.1016/j.jallcom.2023.172981>.
- [22] H. A. Saudi, H. M. H. Zakaly, S. A. M. Issa, H. O. Tekin, M. M. Hessien, Y. S. Rammah, and A. M. A. Henaish. “Fabrication, FTIR, physical characteristics and photon shielding efficacy of CeO_2 /sand reinforced borate glasses: Experimental and simulation studies.”. *Radiation Physics and Chemistry*, **191**:109837, 2022. DOI: <https://doi.org/10.1016/j.radphyschem.2021.109837>.
- [23] H. A. Thabit, A. K. Ismail, H. Es-soufi, D. A. Abdulmalik, A. M. Al-Fakih, S. Alraddadi, and M. I. Sayyed. “Structural, thermal, and mechanical investigation of telluro-borate-bismuth glass for radiation shielding.”. *Journal of Materials Research and Technology*, **24**:4353–4363, 2023. DOI: <https://doi.org/10.1016/j.jmrt.2023.04.082>.
- [24] Phy-X/PSD. “A user friendly online Photon Shielding and Dosimetry (PSD) software. available at <https://phy-x.net/PSD> has been developed for calculation of parameters relevant to shielding and dosimetry.”. , 2023.
- [25] E. Sakar, O. Ozpolat, B. Alim, M. Sayyed, and M. Kurdirek. “Phy-X/PSD: Development of a user friendly online software for calculation of parameters relevant to radiation shielding and dosimetry.”. *Radiation Physics and Chemistry*, **166**:108496, 2020. DOI: <https://doi.org/10.1016/j.radphyschem.2019.108496>.
- [26] XCOM (Photon Cross Sections Database). “NIST XCOM: Element/Compound/Mixture; <https://physics.nist.gov/PhysRefData/Xcom/html/xcom1.html> ”. , 2023.
- [27] H. Akyildirim, E. Kavazb, F. El-Agawany, E. Yousef, and Y. Rammah. “Radiation shielding features of zirconolite silicate glasses using XCOM and FLUKA simulation code.”. *Journal of Non-Crystalline Solids*, **545**:120245, 2020. DOI: <https://doi.org/10.1016/j.jnoncrysol.2020.120245>.
- [28] T. H. Khazaalah, I. S. Mustafa, D. A. Aloraini, R. Hisam, M. H. Mohd Zaid, M. K. Halimah, M. I. Sayyed, M. F. I. A. Malik, A. H. Almuqrin, N. S. Ezra, and H. S. Naeem. “Investigation of optical properties and radioactive attenuation parameters of doped tungsten oxide soda lime silica SLS waste glass.”. *Journal of Materials Research and Technology*, **19**:3355–3365, 2022. DOI: <https://doi.org/10.1016/j.jmrt.2022.05.178>.
- [29] J. Kaewkhao, A. Pokaipisit, and P. Limsuwan. “Study on borate glass system containing with Bi_2O_3 and BaO for gamma-rays shielding materials: Comparison with PbO.”. *Journal of Nuclear Materials*, **399**:38–40, 2010. DOI: <https://doi.org/10.1016/j.jnucmat.2009.12.020>.
- [30] R. Kurtulus, T. Kavas, I. Akkurt, K. Gunoglu, H. O. Tekin, and C. Kurtulus. “A comprehensive study on novel alumino-borosilicate glass reinforced with Bi_2O_3 for radiation shielding applications: synthesis, spectrometer, XCOM, and MCNP-X works.”. *Journal of Materials Science: Materials in Electronics*, **32**:13882–896, 2021. DOI: <https://doi.org/10.1007/s10854-021-05964-w>.
- [31] I. Akkurt, R. Malidarre, and T. Kavas. “Monte Carlo simulation of radiation shielding properties of the glass system containing Bi_2O_3 .”. *European Physical Journal Plus*, **136**:264, 2021. DOI: <https://doi.org/10.1140/epjp/s13360-021-01260-y>.
- [32] B. V. Kheswa. “Gamma radiation shielding properties of $(x)\text{Bi}_2\text{O}_3\text{-(0.5-x)}\text{ZnO-0.2B}_2\text{O}_3\text{-0.3SiO}_2$ glass system.”. *Nukleonika*, **69**:23–29, 2024. DOI: <https://doi.org/10.2478/nuka-2024-0003>.
- [33] R. B. Malidarre, F. Kulali, A. Inal, and A. Oz. “Monte Carlo simulation of a waste soda–lime–silica glass system containing Sb_2O_3 for gamma ray shielding.”. *Emerg. Mater. Res.*, **9**:1334–1340, 2020. DOI: <https://doi.org/10.1680/jemmr.20.00202>.
- [34] M. I. Sayyed, K. A. Mahmoud, O. L. Tashlykov, M. U. Khandaker, and M. R. I. Faruque. “Enhancement of the shielding capability of soda–lime glasses with Sb_2O_3 dopant: A potential material for radiation safety in nuclear installations.”. *Applied Sciences*, **11**:326, 2021. DOI: <https://doi.org/10.3390/app11010326>.

- [35] E. Kavaz, F. E. Agawany, H. Tekin, U. Perisanoglu, and Y. S. Rammah. “Nuclear radiation shielding using barium borosilicate glass ceramics.”. *Journal of Physics and Chemistry of Solids*, **142**:109437, 2020. DOI: <https://doi.org/10.1016/j.jpcs.2020.109437>.
- [36] S. Kaewjaeng, W. Boonpa, S. Kothan, H. J. Kim, C. Jumpee, R. Rajaramakrishna, M. Tungjai, and J. Kaewkhao. “X-ray radiation shielding of CeO₂ doped borosilicate glasses and their luminescence characteristics. ”. *Radiation Physics and Chemistry*, **191**:109825, 2022. DOI: <https://doi.org/10.1016/j.radphyschem.2021.109825>.